Journal of Engineering and Technology for Industrial Applications

ITEGAM-JETIA

Manaus, v.12 n.58, p. 389-398. March/April, 2026.
DOI: https://doi.org/10.5935/jetia.v12i58.3085

ISSN ONLINE: 2447-0228

RESEARCH ARTICLE OPEN ACCESS

EXPERIMENTAL VALIDATION OF A NOVEL DUAL-SLOT SIW BANDPASS FILTER FOR 5G KA-BAND APPLICATIONS

Fatiha Louakhche*[1], Ahcene Abed[2], Redha Bendoumia[3] and Ahmed Bouchekhlal[4]

[1,3]DIC Laboratory, Department of Electronics, Faculty of Technology,University of Blida 1, Blida, Algeria
[2] Electrical Engineering Laboratory (LGE), Department of Electrical Engineering, Faculty of Technology, University of M'sila, M'sila, Algeria
[4] Higher School of Signals (HSS), Kolea, Tipaza, Algeria.

[1]http://orcid.org/0009-0002-6598-930X, [2]https://orcid.org/0000-0002-5089-794X
[3]https://orcid.org/0000-0001-7541-0205, [4]https://orcid.org/0000-0001-5794-6655

E-mail: *louakhche_fatiha@univ-blida.dz, abed.ahcene@univ-msila.dz, bendoumia_redha@univ-blida.dz, bouchekhlalahmed@umc.edu.dz

ARTICLE INFO

Article History
Received: December 8, 2025
Reviewed: January 1, 2026
Accepted: January 14, 2026
Published: March 31, 2026

Keywords:
SIW,
5G,
Ka-band,
mmWave,
Bandpass filter.

ABSTRACT

This study details the design, optimization, and experimental validation of an innovative dual slot Substrate Integrated Waveguide (SIW) bandpass filter intended for 5G Ka-band applications. The proposed filter is implemented on a cost-effective Rogers RO5880substrate and exhibits a second-order quasi elliptic response achieved by etching a novel transverse dual-slot topology within the SIW cavity. The filter was fabricated using standard PCB procedures. The measured results show strong agreement with simulations, confirming the robustness of the design. The small device measures14.15×27.86 mm² and functions effectively inside the 27-29 GHz range, attaining a fractional bandwidth of 8.81%,a return loss of -42 dB, and an insertion loss of -3.16 dB. These results demonstrate that the proposed dual-slot SIW filter provides a highly selective, miniaturized, and low-cost solution, making it a promising candidate for integration in next-generation 5G millimeter-wave front-end systems.

I. INTRODUCTION

Fifth-generation (5G) wireless technology has revolutionized mobile communications, establishing a new paradigm of ultra-low latency, massive machine-type communications, and multi-gigabit data throughput [1], [2]. This enhanced capability is the key enabler for transformative new applications, ranging from autonomous vehicles and intelligent smart cities to immersive augmented and virtual reality experiences [3]. To achieve its promise of high-capacity and multi-gigabit speeds, 5G leverages a wide spectrum, including millimeter-wave (mmWave) frequencies [4]. Within this range, the Ka-band (26.5–29.5 GHz), standardized as bands n257 and n258 in the 3GPP specifications, is particularly critical due to the availability of large contiguous bandwidth blocks, a stark contrast to the more fragmented spectrum below 6 GHz [5], [6]. This abundant bandwidth is the fundamental enabler for the rich user experiences and high-throughput applications envisioned for 5G. However, the deployment of Ka-band relies on dense networks of high frequency small cells, which are ideal for capacity boosting in densely populated urban areas [7], [8].

This architecture is necessary to overcome the significant technical challenges of Ka-band propagation, which is highly susceptible to path loss, atmospheric absorption, and blockage by physical obstacles [9]. Consequently, the development of sophisticated network architectures and supporting technologies is crucial to realizing the potential of Ka-band 5G. The performance of 5G systems in the Ka-band is critically dependent on passive components, particularly filters, which are tasked with signal isolation and interference suppression [10]. A primary design challenge at these high frequencies is minimizing insertion loss to preserve signal integrity, as inherent conductor and dielectric losses become substantial [10]. Furthermore, the architectural shift towards dense small-cell networks and the space constraints within user equipment impose a strict requirement for miniaturization [11]. Consequently, the development of compact filters is not merely an optimization goal but a necessity for enabling the dense and flexible radio designs required for comprehensive 5G coverage.

The drive for widespread adoption also places a premium on economic factors; specifically, 5G requires components that are not only high-performing but also affordable and easy to deploy in large volumes [11]. In this context, low-loss filters provide a dual benefit: they directly improve system efficiency by reducing wasted power and thermal load, and they contribute to the overall cost-effectiveness that is essential for the economic viability of 5G networks [10]. The design of filters for the Ka-band presents a fundamental engineering trade-off. On one hand, traditional waveguide filters are valued for their inherently high-quality factor (Q) and excellent performance at millimeter-wave frequencies [12]. However, their bulky, three dimensional structures render them incompatible with modern planar circuit technologies, severely restricting their integration into compact 5G base stations and user equipment [12]. On the other hand, planar solutions like microstrip filters offer a compact, low-profile form factor that is ideal for integration with standard printed circuit boards (PCBs). Yet, at Ka-band frequencies, these structures suffer from prohibitive conductor losses and significant radiation, which drastically degrades overall system efficiency and performance [13]. This dichotomy creates a critical technological gap. Consequently, there is a pressing need for a filter technology that successfully bridges this divide, merging the low-loss performance of classical waveguides with the compact, planar, and integrable nature of microstrip circuits.

To satisfy the requirement for compact, high-performance filters in 5G and Ka-band applications, SIW technology has emerged as a viable alternative, merging the low-loss and high-Q attributes of traditional waveguides with the benefits of planar integration. SIW structures, often implemented with arrays of metallized vias within a dielectric substrate, provide effective confinement of electromagnetic energy while minimizing radiation losses. By incorporating resonant slots, dual-mode cavities, or defected ground structures (DGS), SIW filters achieve miniaturization and precise frequency selectivity, enabling wide-band, dual band, or quasi-elliptic responses in a compact footprint. Recent designs demonstrate that these techniques allow the realization of high-performance filters with controllable transmission zeros, robust pass-bands, and fabrication compatibility with standard PCB processes, making them highly suitable for 5G base stations and next-generation millimeter-wave consumer devices [14-23]. The primary contribution of this work lies in the design, fabrication, and experimental validation of a novel miniaturized dual-slot SIW bandpass filter specifically optimized for 5G Ka-band applications. The proposed topology innovatively combines inductive metallic posts and precisely engineered transverse dual slots within the SIW cavity, effectively enhancing coupling, generating additional transmission zeros, and improving both selectivity and bandwidth without increasing size.

Implemented on a thin, low-loss Rogers RO5880 substrate, the fabricated filter achieves a compact footprint of 14.15×27.86 mm^2, featuring a low insertion loss of −3.16 dB, FBW of 8.81% at 28 GHz, and an outstanding return loss exceeding −42 dB. These results surpass several recently reported SIW-based filters and confirm the efficiency of the proposed dual-slot configuration. Overall, this work provides a cost-effective, PCB compatible, and high-performance filtering solution that bridges the gap between compact planar integration and waveguide-level quality, making it highly suitable for next-generation millimeter-wave 5G front-end modules. The rest of this paper is structured as follows. A thorough literature overview of recent developments in SIW bandpass filters is given in Section 2, emphasizing their evolution, design techniques, and performance for 5G Ka-band applications. Section 3 introduces the fundamentals of SIW technology, detailing its guiding mechanisms and advantages for millimeter-wave integration. Section 4 describes the materials and methodological approach used in this work, including the design, optimization, and implementation of the proposed slotted SIW BP filter. Section 5 presents and discusses the simulation and experimental results, including the primary SIW waveguide structure, inductive post filter configurations, dual-slot filter design, and experimental validation. The paper is finally concluded in Section 6, which summarizes the key findings and highlighting the practical significance and integration potential of the proposed filter for 5G systems.

II. LITERATURE REVIEW

To meet the size constraints of 5G equipment, researchers have explored miniaturization techniques. Recent studies have demonstrated continuous progress in the development of SIW-based filters to achieve the demanding specifications of 5G and millimeter-wave communication systems. Liao et al. [15] introduced an advanced class of millimeter-wave filters based on a hybrid SIW–spoof surface plasmon polariton (SSPP) and meta structure concepts. Their approach achieved high miniaturization, broad bandwidth, and reduced insertion loss, demonstrating the potential of hybridized SIW platforms for beyond-5G applications. Huang et al. [16] designed a cost-effective substrate-integrated waveguide bandpass filter specifically optimized for 5G bands, providing excellent return loss and high frequency selectivity while maintaining compactness and ease of fabrication. Similarly, Wong et al. [17] proposed a quasi-elliptic SIW filter employing microstrip line cross-coupled resonators and slot-coupled to enhance stopband attenuation and achieve steep skirt selectivity. Moreover, Wang et al. [18] developed a dual-mode bandpass filter based on a slot line resonator structure, offering a compact configuration and wideband response suitable for millimeter-wave frontend integration. Bendahmane et al. [19] proposed a dual-band star-shaped slotted microstrip patch antenna miniaturized using a combination of a high-permittivity substrate and the Defected Ground Structure (DGS) technique.

By replacing the conventional substrate with a high-ε material and introducing carefully designed slots in both the patch and the ground plane, the authors were able to retain dual-band functioning at 2.4 GHz and 5 GHz while significantly reducing the size of the antenna. Sotoodeh et al. (2008) proposed a metallic inductive post-based filter utilizing SIW technology. The filter was designed on the commercial substrate RT/Duroid 5880 with a center frequency of 18.3 GHz. In the passband, the filter response produced less than 2 dB of insertion loss [20]. Additionally, a novel SIW bandpass filter integrating a Defective Microstrip Structure (DMS) and Defective Ground Structure (DGS) and was also proposed [21]. This filter was fabricated on a dielectric material that is 0.5 mm thick and has a dielectric constant of 3.5. It exhibits a stopband attenuation of 28 dB from 26 GHz to 28 GHz and a low insertion loss of 0.5 dB and. For 5G applications, a fractional bandwidth of 7.2% at −3 dB and a center frequency of 27.4 GHz are attained. Zhang et al. (2016) presented a fourth-order Ka-band filter incorporating a negative cross-coupling structure. A coplanar waveguide (CPW) line was used to improve the stopband performance. The proposed design demonstrated greater stopband rejection than a similar fourth-order filter without the CPW line.

The SIW filter was centered at 28 GHz with a bandwidth of 2 GHz [22]. The integration of planar circuits enables the construction of large scale, low-cost microwave and millimeter-wave systems. Designed for 5G millimeter-wave applications, Salehian and Tayarani (2023) presented a dual-pole bandpass filter using a three layer Substrate Integrated Gap Waveguide (SIGGW). The results show that the proposed filter has a single transmission zero close to the passband and an FBW of 5% [23].

III. SIW FUNDAMENTALS

The SIW structure is defined by the upper and lower metal layers of the substrate connected by two parallel rows of metallic via-holes (see Figure 1). The fundamental TE_{10} mode, which is the dominant mode in rectangular waveguides, may propagate because the substrate is essentially sandwiched between these two metal plates [24].

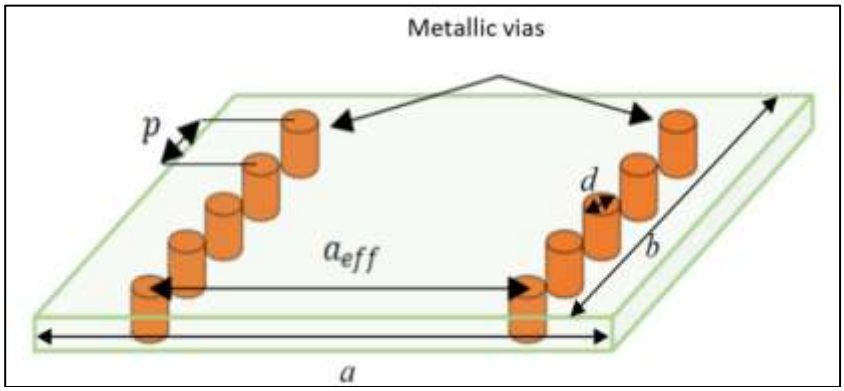

Figure 1: SIW-based structure.
Source: Authors, (2026).

SIW fundamental mode propagation is analogous to that of a rectangular waveguide filled with dielectric and having an equivalent width a_{eff}. The crucial design parameter, the effective width a_{eff}, is obtained from the physical SIW width a, via diameter d, and via pitch p as follows:

$$a_{eff} = a - \frac{d^2}{0.95p} \tag{1}$$

This empirical formula ensures that the SIW cutoff frequency is accurately determined, which is paramount for filter design. The TE_{10} mode's cutoff frequency is:

$$f_c = \frac{c}{2a_{eff}\sqrt{\varepsilon_r}} \tag{2}$$

Where $\varepsilon_r$represents the substrate's relative permittivity, and c denotes the speed of light in vacuum.
The diameter of vias d and the distance between two adjacent$p$are calculated using the following formulas:

$$d \leq \frac{\lambda_g}{5} \tag{3}$$

$$p \leq 2d \tag{4}$$

$\lambda_g$is the wavelength of the waveguide. In the SIW filter for the TE_{10} mode, dimension b is less important because it has no effect on the cut-off frequency of the waveguide. Waveguide bandpass filters can be designed using several methods, including E-planes, H-planes, irises, and metallized cylindrical inductive posts. For SIW technology, metalized cylindrical inductive post filters are particularly advantageous due to their simple implementation [25]. Two approaches are typically used for designing basic inductive post filters: off-centered posts with identical via diameters and centered posts with varying via diameters. Using two symmetrically positioned posts offers distinct advantages over a single post configuration, inherently leading to a smaller spread of higher-order fields for the same susceptance. This is primarily because the symmetrical setup prevents the excitation of the second-order mode. Consequently, this topology allows for optimizing load impedance matching without affecting the susceptance. The susceptance is calculated for the dominant TE_{10} mode, where the electric field vector is directed parallel to the posts, as shown in Figure 2. Deslandes and Wu incorporated the formulas suggested by Gruenberg in their research [24]. The fundamental formulas for this susceptance were derived by analyzing a uniform current in the column and modeling the concentrated currents along its axis to assess the induced fields. Furthermore, it is a standard practice in modern filter synthesis to transform this equivalent network into a *K*-inverter, as defined by Equation (5), to facilitate a systematic design process.

$$K = Z_0 \left| \tan\left(\frac{\phi}{2} + \tan^{-1}\frac{X_a}{Z_0}\right)\right| \tag{5}$$

$$\phi = \tan^{-1}\left(\frac{2X_b}{Z_0} + \frac{X_a}{Z_0}\right) - \tan^{-1}\frac{X_a}{Z_0} \quad (6)$$

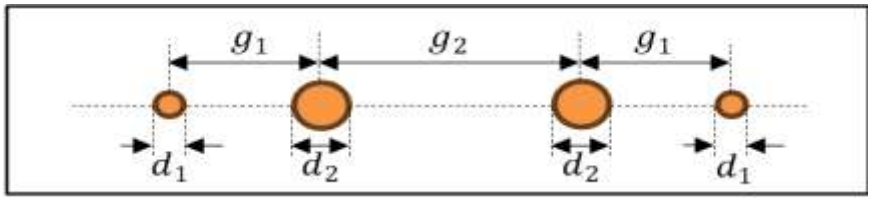

Figure 2: Topology of the centered post-filter model showing various post diameters.
Source: Authors, (2026).

Where: d_1 and d_2 are the diameters of the centered posts, g_1 and g_2 are the distances between them, as shown in Figure 2. Adding slots to SIW structures provides significant design flexibility, enabling the tailoring of the millimeter-wave device's performance for various applications, including 5G communication systems and radar systems.

IV. METHOD AND MATERIALS

The proposed bandpass filter (BPF) presented in Figure 3 is implemented on a Rogers Duroid RO5880 substrate. This material is ideal for high-frequency, broadband applications due to its loss tangent ($tan\ \delta$=0.0009), and relative permittivity εr=2.2.The suggested filter has a frequency of 28 GHz. The recommended filter operates at 28 GHz. To systematically develop the proposed dual-slot BPF, we analyzed the performance of three distinct SIW structures in simulation. First, we began with the SIW Primary Waveguide presented in Figure 3 (a), which serves as the fundamental foundation of the design and exhibits a cutoff frequency near 28 GHz. Next, we investigated the effect of inserting metallic posts to create the SIW Inductive Post Filter (see Figure 3 (b)). This step confirmed the structure's potential as a filter and allowed for initial optimization of the reflection coefficient and insertion loss. Finally, the novel contribution was realized by incorporating a transverse double-slot layout to create the SIW Dual-Slot Filter (see Figure 3 (c)).

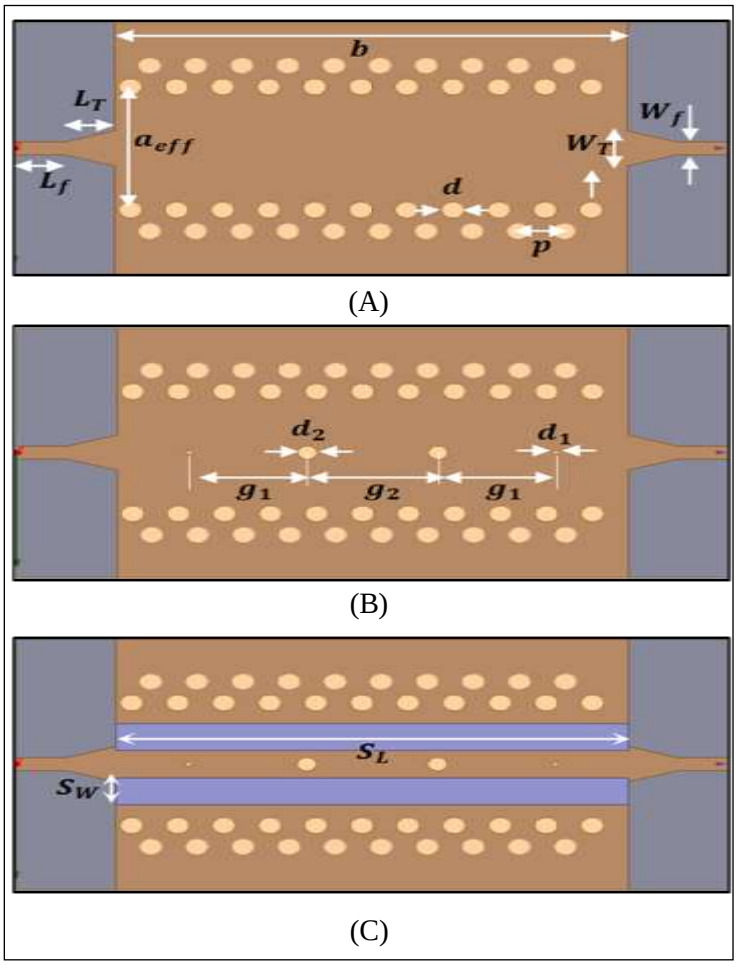

Figure 3: The structures of the proposed 5G filter: a) Basic SIW bandpass filter; b) SIW bandpass inductive post filter; c) SIW bandpass slotted post filter.
Source: Authors, (2026).

To create the micro-strip component, a quarter-wave tapered transformer is connected in series with a 50 Ω microstrip line [26]. The width, W_T, of the tapered line is determined by solving Equation (7), while its length, L_T, is given by Equation (8).

$$\frac{\frac{1}{4.38h}}{\frac{W_T}{h}+1.393+0.667\,ln\left(\frac{W_T}{h}+1.444\right)}=\frac{e^{\frac{-0.627\varepsilon_r}{\frac{\varepsilon_r+1}{2}+\frac{\varepsilon_r-1}{2\sqrt{1+\frac{12h}{W_T}}}}}}{a} \tag{7}$$

$$L_T=\frac{\lambda_g}{4} \tag{8}$$

The wavelength λ_g is given by :

$$\lambda_g=\frac{c}{f_c\sqrt{\varepsilon_r}} \tag{9}$$

First, we used the computationally obtained dimensions to simulate the proposed filter. We then improved it to achieve efficient transmission. The dimensions of the filter, operating at 28 GHz, are mentioned in Table 1.

Table 1: SIW banpass slotted filter parameters.

Parameters	Description	Values (mm)
a_{eff}	SIW width	5,562
p	Space length between adjacent vias	1,8
d	Metal via diameter	0,9
g_1	Post centered diameter	4,62
g_2	Post diameter	5,11
d_1	Distance between two post adjacent	0,22
d_2	Distance between two post adjacent	0,77
W_f	Tapered micro-strip width	0,762
L_f	Tapered micro-strip length	3,92
W_T	Transition width	1,99
L_T	Transition length	1,93
b	SIW length	20
S_L	The length of slots	20
S_W	The width of slots	1,5

Source: Authors, (2026).

V. RESULTS AND DISCUSSION

We used the HFSS simulator to simulate each of the suggested structures. The frequency range is chosen between 26 and 32 GHz. It was found that both the transmission coefficient S12 and the reflection coefficient S11 were measured.

V.1 SIW PRIMARY WAVEGUIDE

We initiated the simulation process with the SIW Primary Waveguide to establish the foundation for the filter design. The electric field distribution shown in Figure 4 validates the fundamental TE_{10} mode's propagation inside the structure. The observed field patterns, characterized by a dominant electric field component perpendicular to the substrate and confined by the metallic via arrays, validate the proper synthesis of the equivalent rectangular waveguide.

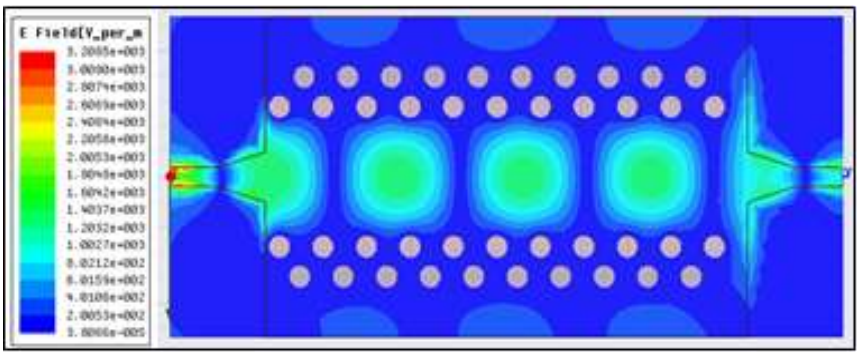

Figure 4: Electric field distribution for the SIW primary waveguide.
Source: Authors, (2026).

Figure 5 illustrates the matching S-parameters of the basic SIW filter. The transmission coefficient S12 is high across the Ka-band, confirming the structure's role as a low-loss transmission medium. More critically, the reflection coefficient S11 exhibits three

distinct resonance minima. These dips occur due to standing wave effects along the length of the waveguide, which contribute to improved impedance matching at those specific frequencies. We note a particularly strong return loss of −46.45 dB at 28.4 GHz, which is vital, as it demonstrates that the basic waveguide structure is already optimally matched at the desired center frequency, providing an excellent starting point for the subsequent filter stages.

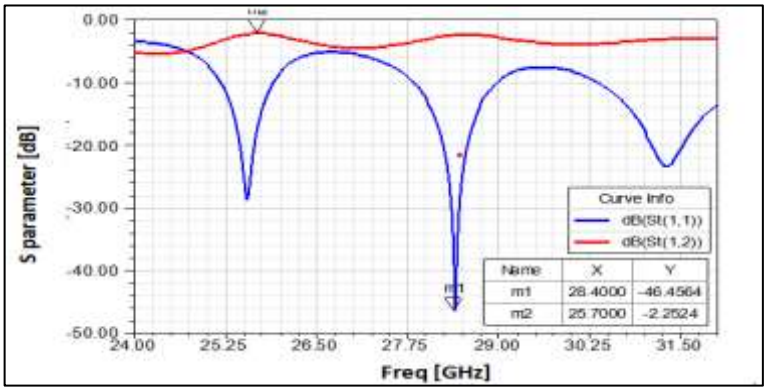

Figure 5: S parameter for the SIW primary waveguide.
Source: Authors, (2026).

V.2 5G BANDPASS FILTER WITH INDUCTIVE POST FILTERS

The next evolutionary step involves integrating inductive metallic posts within the SIW cavity to realize the necessary filtering characteristics. As illustrated in Fig. 6, the insertion of these posts alters the field distribution, effectively creating a series of coupled resonators, forcing the structure to function as a bandpass filter. The metallic posts act as lumped inductive elements, enabling the manipulation of the resonant modes and the establishment of an appropriate inter-resonator coupling mechanism to achieve the desired second-order response.

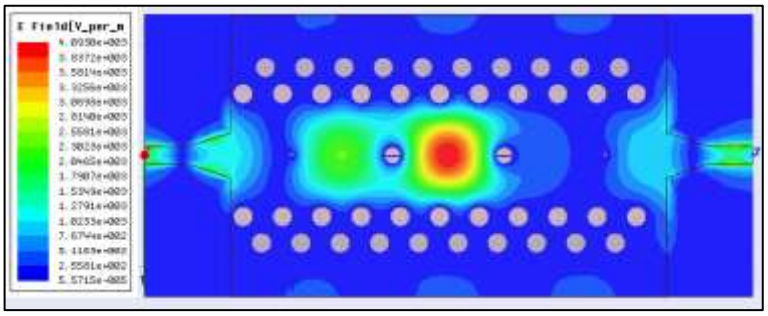

Figure 6: Electric field distribution for the 5G bandpass filter with inductive post filters.
Source: Authors, (2026).

Figure 7 depicts the corresponding simulated S-parameters. The reflection coefficient S11 clearly exhibits a well-defined resonance at the target center frequency of 28 GHz, achieving an excellent impedance matching (return loss) of −31.12 dB. The transmission coefficient S12 confirms the filter functionality, defining a bandwidth that ranges from 27.5 GHz to 28.98 GHz. This results in a desirable fractional bandwidth (FBW) of 5.28%. Furthermore, the filter maintains efficient power transfer within the passband, showing a low insertion loss of −2.71 dB. These results confirm the efficacy of the inductive post topology in synthesizing a functional, low-loss Ka-band filter, providing the required selectivity and initial bandwidth before further enhancement.

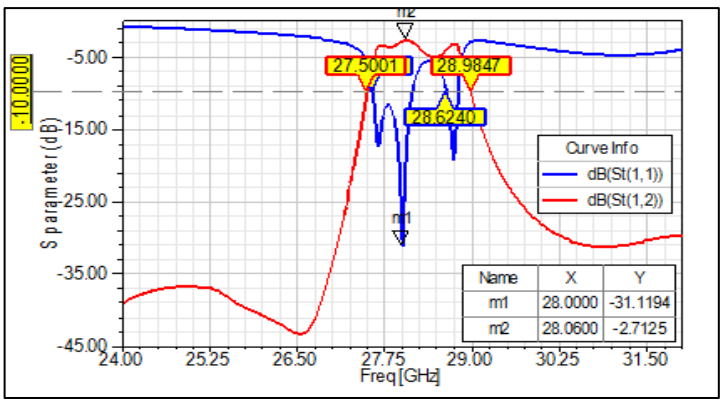

Figure 7: S parameter for the 5G bandpass filter with inductive post filters.
Source: Authors, (2026).

V.3 5G SIW BANDPASS SLOTTED FILTER

Figure 8 illustrates the simulated electric field distribution within the proposed 5G SIW bandpass slotted filter. The field pattern confirms the presence of strong electromagnetic confinement and resonance inside the SIW cavity, particularly around the slot regions, which validates the proposed filtering configuration. This concentrated field distribution demonstrates efficient energy coupling between the input and output ports, ensuring selective transmission at the designed resonant modes.

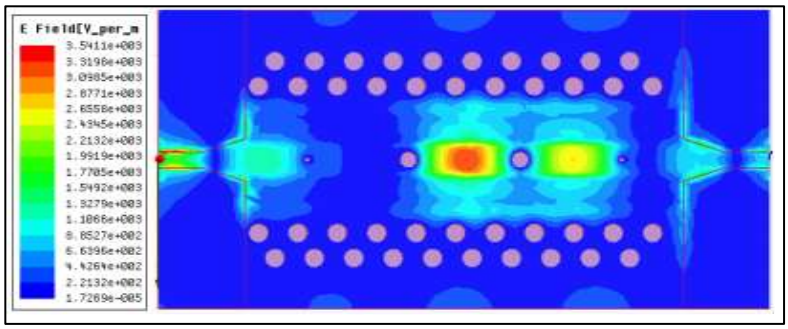

Figure 8: Electric field distribution for the 5G SIW bandpass slotted filter.
Source: Authors, (2026).

As shown in Figure 9, the corresponding S-parameter response reveals the emergence of three distinct resonant frequencies, indicating the excitation of multiple propagation modes within the structure. Among these, the resonance at 28.28 GHz is of primary interest, corresponding to the target 5G Ka−band. At this frequency, the filter exhibits an improved insertion loss of −2.4 dB and a fractional bandwidth (FBW) of 9.04%, representing a clear enhancement compared to the initial configuration. These results confirm that the dual-slot modification significantly improves the bandwidth and transmission efficiency while maintaining compactness, thus validating the effectiveness of the proposed SIW topology for 5G millimeter-wave applications.

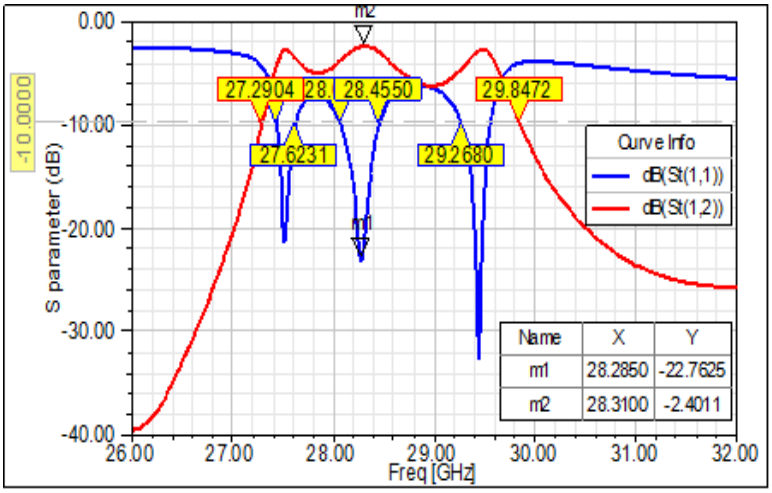

Figure 9: S parameter for the 5G SIW bandpass slotted filter.

V.4 EXPERIMENTAL VALIDATION

As a final step, we put the simulated filter design into practice, and the finished prototype is constructed on a Rogers RO5880 substrate. This substrate has a dielectric constant $\varepsilon_r = 2.2$ and a thickness $h = 0.787\ mm$. Figure 10 shows the 5G SIW bandpass filter's final prototype.

(a) (b)

Figure 10: 5G bandpass SIW filter with double slots: (a) top view;(b) bottom view.
Source: Authors, (2026).

Traditional industrial wave soldering techniques are often complicated and expensive. A simpler and cheaper alternative method is to use solder paste. While this method may affect system performance in some circumstances, we successfully connected the SMA connectors using solder paste. Since the filter is a passive component, the low temperature used during the soldering process did not affect its performance.

The filter's performance was tested using an Agilent PNA-L N5230C network analyzer. The measured S-parameters for the implemented 5G SIW dual-slot filter are shown in Fig. 11, which shows how well it performs in the 25.5 GHz to 30.5 GHz frequency range. Both the transmission (S21) and reflection (S11) coefficients are evident in these results.

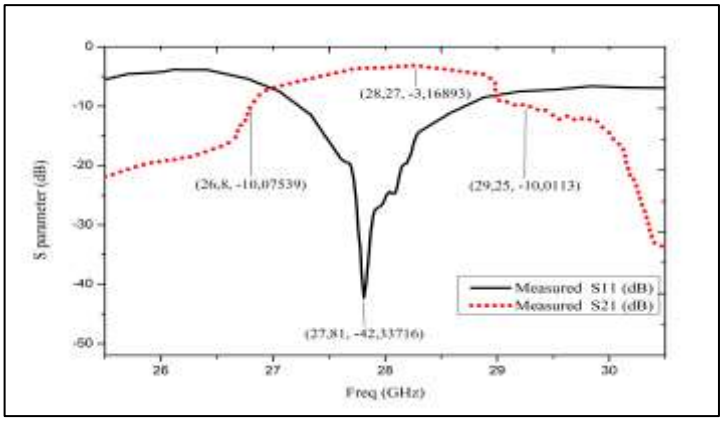

Figure 11: S parameter for the realized 5G SIW bandpass slotted filter.
Source: Authors, (2026).

The transmission coefficient (S21) indicates the filter's minimal loss across its passband, achieving a peak transmission (minimum Insertion Loss) of approximately −3.17 dB at 28.27 GHz. Simultaneously, the reflection coefficient (S11) shows how well the filter is matched to the system impedance, exhibiting a deep minimum (maximum Return Loss) of about −42.34 dB at 27.81 GHz. This very low S11 value confirms an excellent impedance match within the passband. The filter's bandwidth, defined by the −10 dB cutoff points for S21, extends approximately from 26.8 GHz to 29.25 GHz, successfully demonstrating its functionality as a bandpass filter in the designated 5G frequency spectrum. The comparison of the simulated and measured results for the suggested filter is shown in Table 2.

Table2: Simulated and measured results.

/	**Simulated**	**Measured**
FBW(%)	9.04	8.81
RL(dB)	32.7178	42.33
IL(dB)	2.4011	3.16

Source: Authors, (2026).

The comparison between the suggested filter's measured and simulated performance shows an acceptable level of agreement between theory and experiment. The Fractional Bandwidth (FBW) measured at 8.81% is very close to the simulated value of 9.04%, confirming that the operational frequency range was accurately predicted. The filter exhibited an excellent Return Loss (RL), with the measured value of −42.33 dB being significantly better than the simulated −32.72 dB. This superior measured RL indicates an even better impedance match and less reflected power in the physical prototype than anticipated. Conversely, the Insertion Loss (IL) measured at 3.16 dB is higher than the simulated 2.40 dB. This increase in loss is commonly observed in realized prototypes due to real-world factors such as surface roughness, dielectric and conductor losses, and non-ideal SMA connections or soldering, which typically add extra dissipation not perfectly captured in the simulation model.

V.5 COMPARATIVE STUDY

In order to assess the performance of the proposed SIW Bandpass Filter against a number of other SIW BPFs that have been described in the literature employing different technologies, this section conducts a comparative analysis, which is summarized in Table3.

Table3: Comparison between proposed and previously reported bandpass filters.

Ref	$RL(dB)$	$IL(dB)$	$FBW(\%)$	$fc\ (GHz)$
Measured in [21]	20	1.7	7.1	28
Measured in [22]	17	1	3.57	28
Simulated in [23]	60	1.8	5	28
Simulated in [24]	20	0.5	7.2	27.4
Measured in this work	42.33	3.16	8.81	28

(*RL: return loss, *IL: insertion loss, *FBW: -3dB fractional bandwidth, *fC: center frequency)
Source: Authors, (2026).

The comparative study, summarized in Table 3, highlights that the proposed SIW BPF shows good overall performance in the 5G band, particularly excelling in two key criteria: Fractional Bandwidth (FBW) and Return Loss (RL). The filter achieves the highest measured FBW at 8.81%, making it desirable for high-throughput applications by offering the widest relative bandwidth among the compared filters. Furthermore, its measured RL of −42.33 dB is exceptional, being significantly better than all other measured and most simulated results, which confirms the filter's superior impedance matching quality. However, the filter's main drawback is its measured IL=3.16 dB, which is higher than the 0.5 dB to 1.8 dB range reported for the other filters, a difference likely attributable to real-world fabrication losses.

VI. CONCLUSIONS

This work successfully designed, fabricated, and experimentally validated a high performance SIW bandpass filter specifically tailored for operation within the 5G Ka−band. The design leveraged the inherent robustness of the SIW structure and incorporated novel features, including inductive posts and a slotted structure, all progressively optimized in simulation to enhance performance, particularly in terms of bandwidth and impedance matching. The final filter prototype, built on a Rogers RO5880 substrate, was rigorously characterized using an Agilent PNA-L N5230C network analyzer, yielding experimental results that demonstrated strong agreement with the simulations. With an outstanding Return Loss of −42.33 dB, a wide Fractional Bandwidth of 8.81%, and an Insertion Loss of −3.16 dB, the realized filter demonstrates competitive performance centered on 28 GHz. Critically, a comprehensive comparative study with recently published SIW filters confirmed that the proposed design offers superior performance in both its RL and FBW metrics. These strong characteristics position the proposed SIW filter as a highly promising candidate for direct integration into compact and high-performance 5G communication systems. Future work will focus on minimizing Insertion Loss through material optimization and advanced coupling techniques to further enhance the filter's potential for mass production and higher power applications.

VII. AUTHOR'S CONTRIBUTION

Conceptualization: Fatiha Louakhche, Ahcene Abed, Redha Bendoumia and Ahmed bouchekhlal.
Methodology: Fatiha Louakhche and Ahcene Abed.
Investigation: Fatiha Louakhche, Ahcene Abed, Redha Bendoumia and Ahmed bouchekhlal.
Discussion of results: Fatiha Louakhche, Ahcene Abed, Redha Bendoumia and Ahmed bouchekhlal.
Writing – Original Draft: Fatiha Louakhche.
Writing – Review and Editing: Ahcene Abed and Redha Bendoumia.
Resources: Ahcene Abed.
Supervision: Ahcene Abed and Redha Bendoumia.
Approval of the final text: Fatiha Louakhche, Ahcene Abed, Redha Bendoumia and Ahmed bouchekhlal.

VIII. REFERENCES

[1] A. Sukarno, A. Hikmaturokhman and D. Rachmawaty, "Comparison of 5G NR Planning in Mid-Band and High-Band in Jababeka Industrial Estate,"2020 IEEE International Conference on Communication, Networks and Satellite (Comnetsat), Batam, Indonesia, 2020, pp. 12-17, doi: 10.1109/Comnetsat50391.2020.9329000. https://doi.org/10.1109/Comnetsat50391.2020.9329000

[2] C.-P. Li, J. Jiang, W. Chen, Tingfang Ji and J. Smee, "5G ultra-reliable and low-latencysystems design,"in 2017 European Conference on Networks and Communications (EuCNC), Oulu, Finland, 2017, pp. 1-5, https://doi.org/10.1109/EuCNC.2017.7980747

[3] S. Hakak et al., "Autonomous vehicles in 5G and beyond: A survey," *Vehicular Communications*, Vol. 39, p. 100551, 2023,https://doi.org/10.1016/j.vehcom.2022.100551

[4] L. Lianming et al., "The Path to 5G: MmWave Aspects," in Journal of Communications and Information Networks, vol. 1, no. 2, pp. 1-18, Aug. 2016, https://doi.org/10.11959/j.issn.2096-1081.2016.032

[5] Z. Ge, B. You and X. Wen, "Millimeter-wave bandpass filter for 5G-N257 band based on thin-film IPD process," 2023 International Conference on Microwave and Millimeter Wave Technology (ICMMT), Qingdao, China, 2023, pp. 1-3. https://doi.org/10.1109/ICMMT58241.2023.10276743

[6] A. Teber, FR2/mmWave, N258 and N261 Bands, 5G Frequency-Compatible Ultra-Thin Metamaterial Absorber with Polarization Insensitivity for EMI shielding Applications. Adv. Theory Simul. 2024, 7, 2400332. https://doi.org/10.1002/adts.202400332

[7] J. G. Andrews et al., "What will 5G be?" IEEE J. Sel. Areas Commun, vol. 32, no. 6, pp. 1065–1082, Jun. 2014.

[8] D. Liu et al., "User association in 5G networks: A survey and an outlook," IEEE Commun. Surveys Tuts., vol. 18, no. 2, pp. 1018–1044, 2nd Quart., 2016.

[9] X. Lin, "An Overview of 5G Advanced Evolution in 3GPP Release 18," *IEEE Commun. Stand. Mag.*, vol. 6, pp. 77–83, 2022.

[10] K. Shah, "Advancements in 5G Technology: Challenges and Opportunities for Nationwide Deployment," *J. Artif. Intell. CloudComput.*, vol. 1, no. 3, pp. 1–9, 2022, https://doi.org/10.47363/JAICC/2022(1)E203

[11] A. Ichimescu, N. Popescu, E. C. Popovici, and A. Toma, "Energy Efficiency for 5G and Beyond 5G: Potential, Limitations, and FutureDirections," *Sensors*, vol. 24, no. 22, p. 7402, 2024, https://doi.org/10.3390/s24227402

[12] Z. A. Bhat et al., "A Survey on Substrate Integrated Waveguide Filters; Design Challenges and Miniaturizing Techniques for the 5G," Int. J. High Speed Electron. Syst., vol. 32, no. 01, 2023, https://doi.org/10.1142/S0129156421400061

[13] Y. Morimoto, T. Motegi, W. Kasai and K. Niwano, "Transmission Line Loss Properties of Dielectric Loss Tangent and Conductive Surface Roughness in 5G Millimeter Wave Band," 2020 IEEE Asia-Pacific Microwave Conference (APMC), Hong Kong, Hong Kong, 2020, pp. 776-778, https://doi.org/10.1109/APMC47863.2020.9331571

[14] M. Bozzi, "Substrate integrated waveguide (SIW): An emerging technology for wireless systems," 2012 Asia Pacific Microwave Conference Proceedings, Kaohsiung, Taiwan, 2012, pp. 788-790,https://doi.org/10.1109/APMC.2012.6421736

[15] Q. Liao, G. Tang, T. Xiao, C. Liu, L. Huang and H. Wang, " Design of 5G-Advanced and Beyond Millimeter-Wave Filters Based onHybrid SIW-SSPP and Metastructures,"*Electronics*, vol. 14,no. 15, p. 3026, 2025, https://doi.org/10.3390/electronics14153026

[16] J.-M. Huang, H.-T. Xing, and Z.-H. Ma, "Substrate-integrated Waveguide Bandpass Filter for 5G Applications," *Sens. Mater.*, vol. 36, no. 3, p. 1105–1113, 2024, https://doi.org/10.18494/SAM4561

[17] S. W. Wong *et al.* ,"Substrate integrated waveguide quasi-elliptic filter using slot-coupled and microstripline cross-coupled structures," IEEE Transactions on Components, Packaging and Manufacturing Technology, 2016, vol. 6, no. 12, p. 1881–1888. https://doi.org/10.1109/TCPMT.2016.2625744

[18] Q. Wang, R. Xiao, G. Yang and W. Wu, "A Novel Compact Wide-Band Dual-Mode Bandpass Filter with Slotline Resonator," 2018 International Conference on Microwave and Millimeter Wave Technology (ICMMT), Chengdu, China, 2018, pp. 1-3, https://doi.org/10.1109/ICMMT.2018.8563296

[19] Z. Bendahmane, S. Ferouani, and Ch. Sayah, "High Permittivity Substrate and DGS Technique for Dual-Band Star-Shape Slotted Microstrip Patch Antenna Miniaturization,"Progress In Electromagnetics Research C, Vol. 102, 163-174, 2020, https://doi.org/10.2528/PIERC20021501

[20] Z. Sotoodeh, B. Biglarbegian, F. Hojjat-Kashani, and H. Ameri Mahabadi,"A Novel Bandpass Waveguide Filter Structure on SIW Technology," Progress In Electromagnetics Research Letters, Vol. 2, 141-148, 2008, https://doi.org/10.2528/PIERL08010204

[21] P.A. Banu and H.H. Umma, "Design of SIW Bandpass Filter using DGS-DMS Technique for 5G Application," Journal of Analog and Digital Communications, vol. 3, no. 3, pp. 1-6, 2018.

[22] D. Zhang, P. Zhou, Z. Yu and J. Zhou, "Ka-band quadruple SIW filter with controllable transmission zeros," 2016 IEEE International Conference on Microwave and Millimeter Wave Technology (ICMMT), Beijing, China, 2016, pp. 296-298, https://doi.org/10.1109/ICMMT.2016.7761753.

[23] K. Salehian and M. Tayarani," A novel SIGGW dual post band-pass filter for 5G millimeter-wave band applications with a transmission zero," Sci Rep 13, 20743 (2023). https://doi.org/10.1038/s41598-023-47490-1

[24] D. Deslandes and K. Wu, "Single-substrate integration technique of planar circuits and waveguide filters," IEEE Transactions on Microwave Theory and Techniques, vol. 51, no. 2, pp. 593-596, Feb. 2003, https://doi.org/10.1109/TMTT.2002.807820

[25] Y. M. Huang et al., "Half-mode substrate integrated waveguide bandpass filter loaded with horizontal–asymmetrical stepped-impedance complementary split-ringresonators," *Electron. Lett.*, vol. 52, no. 12, pp. 1034–1036, 2016, https://doi.org/10.1049/el.2016.0372

[26] A. Abed, A. Bouchekhlal, A. Amrouche, and R. Bendoumia, "Low-cost cband siw bandpass filter using fr4-epoxy substrate," Jordanian Journal of Computers and Information Technology (JJCIT), vol. 09, no. 02, pp. 166–174, 2023.